LAYOUT OPTIMIZATION FOR MAXIZING WIND FARM POWER PRODUCTION USING SEQUENTIAL CONVEX PROGRAMMING

Jinkyoo Park and Kincho H. Law

Department of Civil and Environmental Engineering,

Stanford University, Stanford, CA, USA.

Email: law@stanford.edu

ABSTRACT

This paper describes an efficient method for optimizing the placement of wind turbines to maximize the expected wind farm power. In a wind farm, the energy production of the downstream wind turbines decreases due to reduced wind speed and increased level of turbulence caused by the wakes formed by the upstream wind turbines. As a result, the wake interference among wind turbines lower the overall power efficiency of the wind farm. To improve the overall efficiency of a wind farm, researchers have studied the wind farm layout optimization problem to find the placement locations of wind turbines that maximize the expected wind farm power. Most studies on wind farm layout optimization employ heuristic search-based optimization algorithms. In spite of their simplicity, optimization algorithms based on heuristic search are computationally expensive and have limitation in optimizing the locations of a large number of wind turbines since the computational time for the search tends to increase exponentially with increasing number of wind turbines. This study employs a mathematical optimization scheme to efficiently and effectively optimize the locations of a large number of wind turbines with respect to maximizing the wind farm power production. To formulate the mathematical optimization problem, we derive a continuous wake model and express the expected wind farm power as a continuous and smooth function in terms of the locations of the wind turbines. The constructed wind farm power function is then maximized using sequential convex programming (SCP) for the nonlinear mathematical problem. We show how SCP can be used to evaluate the efficiency of an existing wind farms and to optimize the wind farm layout consisting 80 wind turbines.

1. INTRODUCTION

Among the various renewable energy sources, wind power has proven effective for large-scale energy production. However, for a large-scale wind farm, wind power production efficiency can deteriorate due to wake interference among the wind turbines. Wakes formed by the upstream wind turbines affect the wind speed behind their rotor and decrease the energy production of the downstream wind turbines due to reduced wind speed and increased level of turbulence. The relative locations of the wind turbines affect the wake interference pattern among the wind turbines and, thus, the energy production. In this paper, we discuss a method for improving the expected wind farm power by strategically placing the wind turbines in a wind farm site.

To improve the energy production of a wind farm as a whole, the locations of wind turbines need to be strategically determined. The wind farm layout optimization problem can be formulated to maximize the expected wind farm power (objective function) in terms of the locations (optimization variable) of wind turbines. To construct the expected wind farm power function, a wake model, an analytical expression of the wind speed after a wind turbine, is required. Wake is often described by its domain (shape) and value (in terms of ratio of wind speed reduction). For example, the Park wake model assumes the wake expands linearly as it propagates in the downstream direction; the wind speed inside the wake (3D expansion cone) is assumed constant whose value is a fraction of the wake-free wind speed (Jensen, 1986; Katic *et al.,* 1986). For the Park wake model, the wake profile is compactly expressed as a piece-wise linear function. Due to its simplicity, the model has been widely used in many wind farm power evaluation software, such as WAsP (Risø, 2011), WindFarmer (DNV GL, 2014), WindPRO (EMD International, 2011) and OpenWind (AWS Truepower, LLC, 2008).

The use of a piece-wise linear function for the Park wake model results in a non-smooth (non-differentiable) wind farm power function, which renders optimizing the wind farm power function using gradient-based optimization algorithms difficult. Various heuristic optimization algorithms have been deployed to solve the wind farm layout problem. For example, genetic algorithms (GAs) have been used to optimize the locations of wind turbines (Mosetti *et al*., 1994; Grady *et al*., 2004; Kusiak *et al.,* 2010; Elkinton, *et al.,* 2010; Serrano *et al.,* 2010). The efficiency of GA algorithms strongly depends on the discretization of the search space; a fine discretisation for the search space

would improve the effectiveness on finding optimal solution but also would incur significant computational cost. Optimization algorithms based on stochastic search (sampling), such as Particle Swarm Optimization (Wan *et al.*, 2012, Chowdhury *et al.,* 2012; Chowdhury *et al.,* 2013), Simulated Annealing (Bilbao and Alba, 2009), Monte Carlo Simulation (Marmidis *et al.,* 2008), Extended Pattern Search (EPS) (Du Pont and Cargan, 2012), Ant Colony algorithm (Eroglu and Seckiner*,* 2012) and Coral Reefs Optimization algorithm (Salcedo-Sanz *et al.,* 2014) have also been deployed. Although these algorithms are simple and are efficient for small-scale optimization problems, they are not effective for solving the wind farm layout problem with a large number of wind turbines due to the computational cost necessary to search in a high dimensional input space.

In this study, we derive a continuous and smooth wind speed profile that would allow the wind farm power function to be expressed as a smooth (differentiable) function of wind turbine location variables. The wind farm power function can then be efficiently optimized using a gradient-based optimization algorithm even for a wind farm with a large number of wind turbines. CFD simulations and wind tunnel experimental studies have shown that a wind speed profile inside a wake resembles an inverted Gaussian shape, showing a continuous variation in wind speed in both the downstream and the radial direction (Ainslie, 1988; Bartl *et al.,* 2011). We therefore propose the use of a continuous wake model to represent the wind speed variation inside the wake using a smooth and continuous function in both the wake downstream and radial directions. We then apply sequential convex programming (SCP) to maximize the wind farm power. SCP, through iterative approximations, can effectively optimize the non-convex wind farm power function. We derive the gradient of the objective function, which is required for SCP, and show how SCP can be used to evaluate the efficiency of existing wind farms as well as to design layout of a wind farm for maximizing the power production at a target site.

This paper is organized as follows: first, we derive the wind farm power function constructed using a continuous wake model. The derived wind farm power function is then calibrated using CFD simulation data. The wind farm layout optimization problem is then formulated and solved by applying sequential convex programming. The proposed optimization approach is used to evaluate the efficiency of an operating wind farm and to study the optimal layout of a wind farm. Finally, the paper is concluded with a summary and discussion.

2. DERIVATION OF WIND FARM POWER FUNCTION

This section describes the derivation of a wind farm power function to be used as the objective function for the wind farm layout optimization problem. The wind farm power function is derived as follows: The power expression for a single wind turbine, under undisturbed wind flow condition, is described based on the actuator disc model in aerodynamics. A continuous wake model to represent the wind speed profile behind a wind turbine is then discussed. The power of a downstream wind turbine under the influence of *a single wake* formed by a single upstream wind turbine is derived based on momentum conservation theory. The power of a downstream wind turbine under the influence of *multiple wakes* caused by upstream wind turbines is constructed by aggregating the energy deficiencies due to wakes. Finally, the wind farm power function is expressed as the sum of the powers of all the wind turbines in a wind farm.

2.1 Power function of a wind turbine

The power of a single wind turbine due to a wind flow with wind speed U can be obtained based on the actuator disc model in aerodynamics (Burton, 2001). According to the actuator disc model, the wind turbine power can be quantified by the amount of power extracted by the disc that represents the rotor of the wind turbine. The model defines an induction factor $\alpha = (U - U_R)/U$, where U and U_R are, respectively, the wind speed of the free stream and the wind speed right behind the rotor disc, to quantify the wind speed reduction passing through the rotor disc. The wind turbine power P can then be expressed as a function of U and α as (Burton, 2001):

$$P = \frac{1}{2}\rho A U^3 4\alpha(1-\alpha)^2 \tag{1}$$

where ρ and A are the air density and the rotor area, respectively. To relate the induction factor α and the efficiency of power extraction, the power coefficient C_P representing the ratio between the extracted power and the available wind flow energy $\rho A U^3/2$ at the disc is defined as (Burton, 2001):

$$C_P(\alpha) = \frac{P}{\rho A U^3/2} = 4\alpha(1-\alpha)^2 \tag{2}$$

Note that C_P, which is a function of the induction factor α, has the maximum value of $C_P^* = 16/27$ when $\alpha = 1/3$. The maximum value C_P^* is known as s Betz's coefficient, a ratio of the maximum energy extractable by an idealized rotor disc to the wind flow kinematic energy (Betz, 1966).

A modern large-scale wind turbine regulates the power output by controlling the induction factor α through autonomous adjustments in the blade pitch angles or the blade tip speed ratio $\omega R/U$, where ω and R are the rotor angular speed and rotor radius, respectively. When the wind speed is less than the cut in wind speed U_{in}, the wind turbine is parked stationary without generating energy due to insufficient wind flow energy to overcome the mechanical and electrical resistance. Above the cut in wind speed U_{in} and below a cut out wind speed U_{out}, the wind turbine would try to adjust the induction factor $\alpha = 1/3$ to maximize its power output as given in Eq. (1). To maintain $\alpha = 1/3$, a wind turbine adjusts the blade tip speed ratio by changing the generator's load (i.e., torque). When the wind speed is over the cut out wind speed U_{out}, the wind turbine shifts the induction factor α from its optimum $\alpha = 1/3$ to lower or higher value to maintain a constant level of power for the higher wind speed, thereby protecting the generator and the mechanical components of the wind turbine from excessive electrical as well as structural loads. Therefore, the power of a controlled wind turbine can be expressed as (Yaw, 2010):

$$P(U) = \begin{cases} 0, & \text{if } U < U_{in} \\ \frac{1}{2}\rho A C_P^* U^3, & \text{if } U_{in} \le U < U_{out} \\ \frac{1}{2}\rho A C_P(\alpha) U^3 = \frac{1}{2}\rho A C_P^* U_{out}^3, & \text{if } U_{out} \le U \end{cases} \tag{3}$$

Typical values for the cut in wind speed U_{in} and the cut out wind speed U_{out} are 3 m/s and 12m/s, respectively. When $U \ge U_{out}$, $C_P(\alpha)$ is adjusted to keep the the clipped wind turbine power $(1/2)\rho A C_P^* U_{out}^3$, generally referred as the rated power. In this paper, it is assumed that all wind turbines follow this conventional control method. We change only the locations of wind turbines so that the wind turbines can face more favorable (i.e., less-wake affected) wind flow.

2.2 Wake profile model

The interaction between wind flow and the rotating blades of a wind turbine generates turbulent wind flow, called a wake, resulting in non-uniform wind speed profile behind the wind turbine. A wake has been mathematically described in terms of both its domain (shape) and value (as the ratio of wind speed reduction). One of the most prevalent wake models is the Park wake model (Jensen, 1986; Katic *et al.,* 1986), which expresses the wind speed at the downstream-wake distance d and the radial-wake distance r in the wake formed behind the upstream wind turbine with an induction factor of α as

$$u(d,r) = \big(1 - \delta u(d,r,\alpha)\big)U \tag{4}$$

where $\delta u(d,r,\alpha)$ is termed the wind speed deficit factor that quantifies how much the wind speed at (d,r) is reduced by the wake. As shown in Figure 1, the Park wake model assumes that the radius of the wake increases linearly with the downstream distance d as $R(d) = R_0 + \kappa d$, where R_0 is the radius of the wind turbine rotor and κ is the wake expansion rate determined by the surface roughness of a site. Furthermore, for the Park wake model, the wind speed is assumed uniform inside the wake with the wind speed deficit factor $\delta u(d,r,\alpha)$ expressed as (Jenson, 1986):

$$\delta u(d,r,\alpha) = \begin{cases} 2\alpha\left(\dfrac{R_0}{R(d)}\right)^2, & \text{if } r \le R(d) \\ 0, & \text{if } r > R(d) \end{cases} \tag{5}$$

Note that the wind speed abruptly changes at the boundary of the wake region, corresponding to the boundary surface of a 3-D cone whose radius is $R(d) = R_0 + \kappa d$.

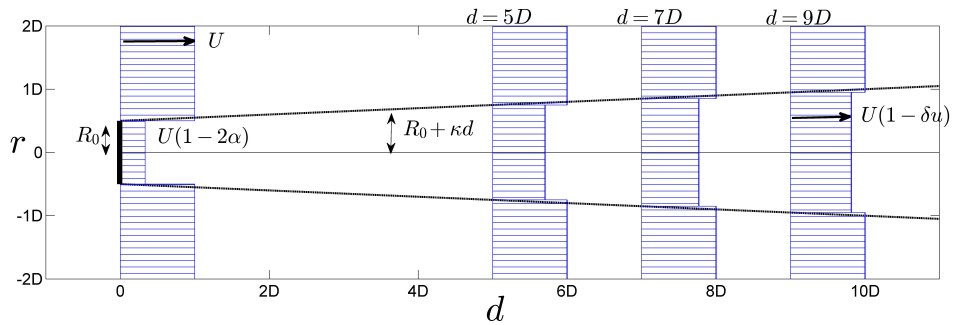

Figure 1. Wind speed profile described using the Park wake model.

It has been observed that when a wake propagates beyond a distance of about five times the rotor's diameter ($d > 5D$), the cross sectional wind speed profile closely resembles an inverted Gaussian function (Ainslie, 1988; Bartl *et al.,* 2011). To construct the wind farm power function while accounting for realistic wake effect, we express the deficit factor $\delta u(d, r, \alpha)$ as

$$\delta u(d, r, \alpha) = s(d, \alpha) \exp\left(-\left(\frac{r}{R(d)}\right)^2\right) \tag{6}$$

In Eq. (6), the decrease of the deficit factor with the downstream distance d is captured by the scaling function $s(d, \alpha)$, while the decrease with the radial distance r is depicted by the exponential function $\exp(-(r/R(d))^2)$. The continuous wake model function, as shown in Figure 2, varies smoothly at the boundary of a wake by the relative magnitude between r and the wake radius $R(d)$ at the downstream distance d.

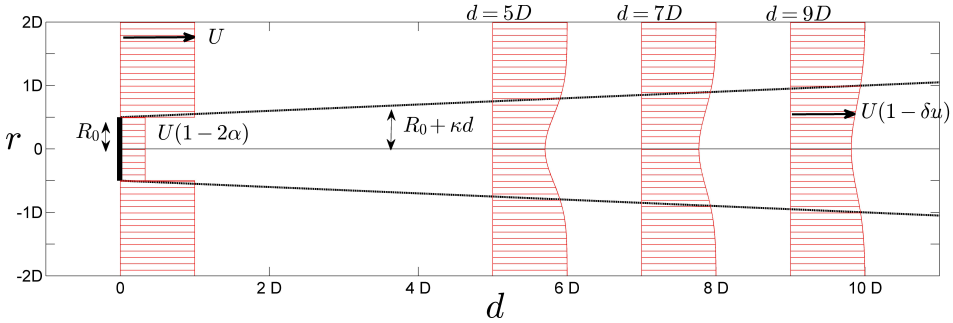

Figure 2. Wind speed profile described using the continuous wake model.

The scaling function $s(d,\alpha)$ can be derived based on the momentum conservation at the two points located, respectively, right behind the rotor and at the downstream distance d as

$$U(1-2\alpha)A(0) = \int_{A(d)} U\big(1-\delta u(d,r,\alpha)\big)\, U dA(d) \tag{7}$$

Substituting the expression of the deficit factor $\delta u(d,r,\alpha)$ in Eq. (6) into Eq. (7), the scaling function $s(d,\alpha)$ can be determined as

$$\begin{aligned} s(d,\alpha) &= 2\alpha A(0) \Big/ \int_{A(d)} \exp\left(-\left(\frac{r}{R(d)}\right)^2\right) dA(d) \\ &= 2\alpha\pi {R_0}^2 / 2\pi \int_{r=0}^{r=\infty} \exp\left(-\left(\frac{r}{R(d)}\right)^2\right) r dr \\ &= \alpha {R_0}^2 \Big/ \left[-\frac{R(d)^2}{2}\exp\left(-\left(\frac{r}{R(d)}\right)^2\right)\right]_{r=0}^{r=\infty} \\ &= 2\alpha\left(\frac{R_0}{R(d)}\right)^2 \end{aligned} \tag{8}$$

Note that this scaling function is the same as wind speed deficit factor in the Park wake model when the radial distance $r \le R(d)$. Finally, substituting the expression for the scaling function $s(d,\alpha)$ into Eq. (6), the deficit factor at (d,r) behind an upstream wind turbine with an induction factor of α can be expressed as

$$\delta u(d,r,\alpha) = 2\alpha\left(\frac{R_0}{R(d)}\right)^2 \exp\left(-\left(\frac{r}{R(d)}\right)^2\right) \tag{9}$$

Figure 2 shows the wind speed profile described by Eq. (9) with a linear wake expansion curve $R(d) = R_0 + \kappa d$. As shown in the figure, the wind speed recovers (i.e., the deficit factor decreases) as d and r increase. Furthermore, the wake region is described by a smooth and continuous function as defined by Eq. (9). The smooth and continuous function describing the wake profile facilitates the modelling of wake interactions among multiple wind turbines in a wind farm. Furthermore, the continuous wake model allows employing gradient-based optimization algorithms to efficiently determine the locations of wind turbines that maximize the total power production in a wind farm.

2.3 Wind turbine power accounting for a single wake

Using the expression for the power of a single wind turbine under wake-free wind flow condition and the expression for the wind speed profile inside a wake, the power output P_{ij} of a downstream wind turbine i due to the wake formed by an upstream wind turbine j can be derived. Given the wind direction θ^W and the locations of two wind turbines i and j, denoted as $l_i = (x_i, y_i)$ and $l_j = (x_j, y_j)$ as shown in Figure 3, the downstream wake inter distance d_{ij} and the radial wake inter distance r_{ij} between the hubs of wind turbines i and j can be determined, respectively, as

$$d_{ij} = \|l_i - l_j\|_2 \cos(|\theta_{ij} - \theta^W|) \tag{10-a}$$

$$r_{ij} = \|l_i - l_j\|_2 \sin(|\theta_{ij} - \theta^W|) \tag{10-b}$$

where $\|l_i - l_j\|_2 = \left((x_i - x_j)^2 + (y_i - y_j)^2\right)^{1/2}$ and $\theta_{ij} = \tan^{-1}\left((x_i - x_j)/(y_i - y_j)\right)$ are, respectively, the inter distance and the angle between the two wind turbines i and j. The downstream wake inter distance d_{ij} and the radial wake inter distance r_{ij} play an important role in modelling wind turbine power under wake influence.

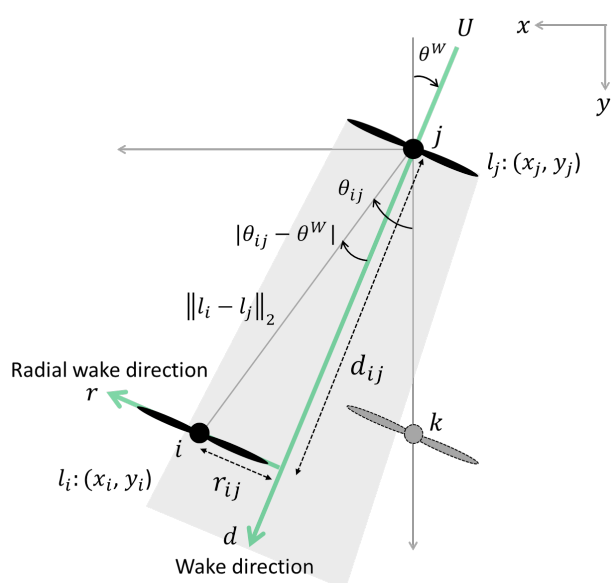

Figure 3. Mapping the relative locations to the wake downstream distance d_{ij} and radial distances r_{ij}.

As shown in Figure 4(a), with d_{ij} and r_{ij}, the wind speed profile on the rotor disc of the downstream wind turbine i can be computed. Using the local polar coordinate (r', θ') as shown in Figure 4(b), we determine the wind speed at any arbitrary location on the rotor disc of the downstream wind turbine i. That is, the wind speed u_{ij} at (r', θ') of the downstream wind turbine i due to the wake caused by the upstream wind turbine j for the free stream wind speed U and wind direction θ^W can be determined by substituting $d = d_{ij}$ and $r = \sqrt{\left(r_{ij} - r'\cos\theta'\right)^2 + (r'\sin\theta')^2}$ into Eq. (9) as

$$u_{ij}\left(r', \theta', l_i, l_j; U, \theta^W\right) = \begin{cases} U\left(1 - \delta u\left(d_{ij}, r, \alpha_j\right)\right), & \text{if } d_{ij} \geq 0 \\ U & , \text{ otherwise} \end{cases} \tag{11}$$

Only when wind turbine i is located at the downstream, i.e., $d_{ij} \geq 0$, would the turbine experiences the wake affected wind speed $U\left(1 - \delta u\left(d_{ij}, r, \alpha_j\right)\right)$; otherwise wind turbine i experiences the non-reduced wind speed U. Note that d_{ij} and r are functions of the location variables $\left(l_i, l_j\right)$ as well as the wind direction θ^W.

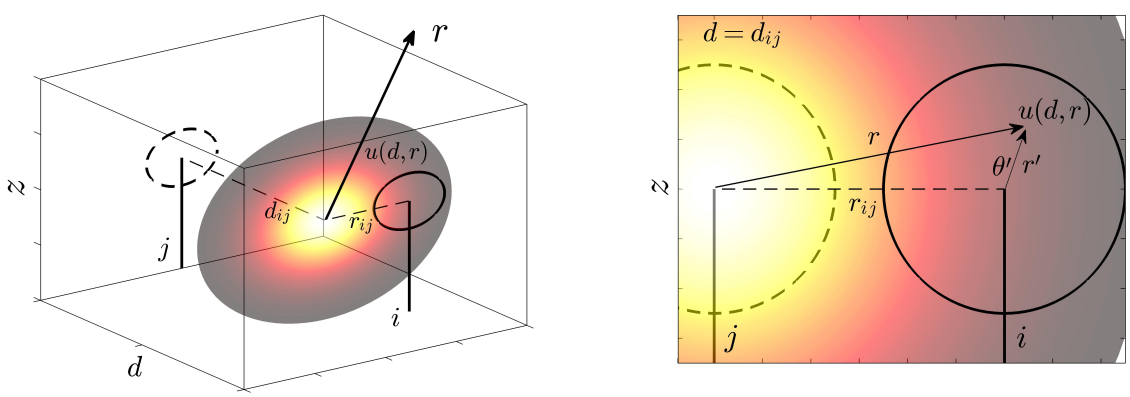

(a) Wind speed profile in the global polar coordinate

(b) Wind speed profile mapped on the local polar coordinate

Figure 4. Wind speed profile experienced by the downstream wind turbine i inside the wake formed by the upstream wind turbine j

Once the wind speed profile on the rotor of the wind turbine is determined, the power can be determined by simply integrating the power on every location (r', θ') on the rotor area. For the purpose of aggregating wake influences by

multiple wind turbines to be discussed in the next section, here we derive the averaged wind speed $\bar{u}_{ij}$ on the rotor disc of the downstream wind turbine i due to the wake by the upstream wind turbine j. From conservation of momentum, we set the momentum acting on the rotor disc due to the averaged wind speed $\bar{u}_{ij}$ equal to the momentum acting on the same rotor disc due to the varying wind speed u_{ij}, i.e., $\bar{u}_{ij}A_{rotor} = \int_{A_{rotor}} u_{ij} dA_{rotor}$. Therefore, the average wind speed $\bar{u}_{ij}$ can be expressed as

$$\bar{u}_{ij}\left(l_i, l_j; U, \theta^W\right) = \frac{1}{\pi R_0^2} \int_{\theta'=0}^{\theta'=2\pi} \int_{r'=0}^{r'=R_i} u_{ij}\left(r', \theta', l_i, l_j; U, \theta^W\right) r' dr' d\theta' \tag{12}$$

where the integration over the rotor disc area is conducted using the polar coordinates (r', θ'). The average wind speed $\bar{u}_{ij}$ of the wind turbine i due to the wind turbine j, given the wind speed U and the wind direction θ^W, is expressed as a function of the locations of the two wind turbines i and j. Then, the power P_{ij} of the downstream wind turbine i due to the wake formed by the upstream wind turbine j can be found by substituting $\bar{u}_{ij}\left(l_i, l_j; U, \theta^W\right)$ shown in Eq. (12) in place of U in Eq. (3).

2.4 Wake interference model among multiple wind turbines

In a wind farm, multiple wakes formed concurrently by upstream wind turbines affect the power of a downstream wind turbine. For taking multiple wakes into account, various methods have been proposed and implemented in wind farm power prediction software. A comparison study on the different ways in accounting for multiple wakes has been reported by Bartl (2011). One widely used method is based on the conservation of kinetic energy proposed by Katic *et al.* (1986). This model assumes that the kinetic energy deficit by the mixed wake equals the sum of the kinetic energy deficits by individual wakes. The deficit factor for the downstream wind turbine i is determined by aggregating all the averaged deficit factors $\delta\bar{u}_{ij} = 1 - \bar{u}_{ij}/U$, defined between the wind turbine i and the wind turbines $\{j | \boldsymbol{W}_{(i,j)} = 1\}$ that influence the wind turbine i (Katic *et al.,* 1986) :

$$\delta\bar{u}_i(\boldsymbol{l};\theta^W) = \sqrt{\sum_{\{j|\boldsymbol{W}_{(i,j)}=1\}} \left(\delta\bar{u}_{ij}\right)^2} \tag{13}$$

where the Boolean wake influencing matrix $\boldsymbol{W}$ describes how the wind turbines interfere each other with wakes under the wind direction of θ^W. With the Park wake model, the (i,j)th entry of $\boldsymbol{W}$ is set as 1 if the wind turbine j influences wind turbine i based on the definition of the wake region $d \leq R(d)$ in Eq. (5); otherwise it is set to zero.

For the continuous wake model, based on the expressions for u_{ij} and $\bar{u}_{ij}$ in Eqs. (11) and (12), the averaged deficit factor $\delta\bar{u}_{ij} = 1 - \bar{u}_{ij}/U$ for the downstream wind turbine i affected by the upstream wind turbine j can be expressed as

$$\delta\bar{u}_{ij}(l_i, l_j; \theta^W) = \begin{cases} \dfrac{1}{\pi R_i^2} \displaystyle\int_{\theta'=0}^{\theta'=2\pi} \int_{r'=0}^{r'=R_i} \delta u(d_{ij}, r, \alpha_j) r' dr' d\theta' , & \text{if } d_{ij} \geq 0 \\ 0 , & \text{otherwise} \end{cases} \tag{14}$$

Furthermore, since the continuous wake model has the wake width expanding indefinitely, as shown in Figure 5, all the upstream wind turbines affect the downstream wind turbine i. Therefore, the aggregated deficit factor $\delta\bar{u}_i(\boldsymbol{l};\theta^W)$ for wind turbine i can be generalized without using the Boolean wake influencing matrix $\boldsymbol{W}$ as

$$\delta\bar{u}_i(\boldsymbol{l};\theta^W) = \sqrt{\sum_{j=1}^{N_T} \left(\delta\bar{u}_{ij}(l_i, l_j; \theta^W)\right)^2} \tag{15}$$

Note that the aggregated deficit factor for wind turbine i is expressed as a function of $\boldsymbol{l} = (l_i, \dots, l_{N_T})$, the locations of the N_T wind turbines in a wind farm, where $l_i = (x_i, y_i)$.

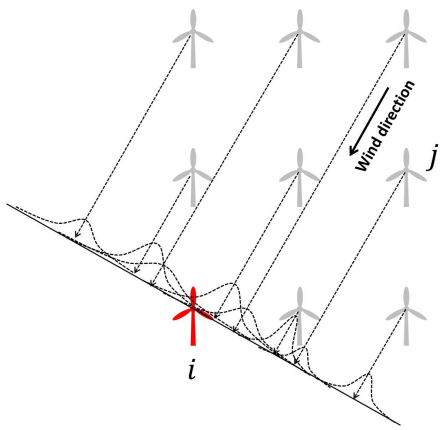

Figure 5. Influence of wakes from upstream wind turbines on downstream wind turbine i

Given the wind condition (U, θ^W), from Eq. (4), the average wind speed $\bar{u}_i$ experienced by the downstream wind turbine i can be expressed as

$$\bar{u}_i(\boldsymbol{l}; U, \theta^W) = (1 - \delta\bar{u}_i(\boldsymbol{l}; \theta^W))U \tag{16}$$

Substituting the wind speed $\bar{u}_i(\boldsymbol{l}; U, \theta^W)$ into Eq.(3), the power P_i of wind turbine i can be expressed in terms of the locations $\boldsymbol{l}$ of all the wind turbines in a wind farm as

$$P_i(\boldsymbol{l}; U, \theta^W) = \begin{cases} 0, & \text{if } \bar{u}_i(\boldsymbol{l}; U, \theta^W) < U_{int} \\ \frac{1}{2}\rho A C_P^* \bar{u}_i^3(\boldsymbol{l}\,; \theta^W, U), & \text{if } U_{in} \le \bar{u}_i(\boldsymbol{l}; U, \theta^W) < U_{out} \\ \frac{1}{2}\rho A C_P^* U_{out}^3, & \text{if } U_{in} \le \bar{u}_i(\boldsymbol{l}; U, \theta^W) \end{cases} \tag{17}$$

where $C_P^* = C_P(\alpha = 1/3) = 16/27$, the maximum power coefficient. Finally, given the wind speed U and the wind direction θ^W, the wind farm power can be computed by summing the power productions of the N_T wind turbines in the wind farm as $\sum_{i=1}^{N_T} P_i(\boldsymbol{l}; U, \theta^W)$.

3. CALIBRATING WIND FARM POWER FUNCTION WITH CFD SIMULATION DATA

The wind farm power function derived in the previous section is based on the continuous wake model, in which the wind speed profile is described by the wake expansion rate κ, such that the wake radius at a downstream distance d is defined as in $R(d) = R_j + \kappa d$. To determine the wake expansion rate κ, one approach is to employ CFD simulation data on the wind speed profile inside the wake. Additionally, we compare the wind farm power function with the simulation code to assess our model.

3.1 CFD simulation

To determine the wake expansion parameter κ, we use the CFD simulation data generated using a high-fidelity CFD tool, called SOWFA Super-Controller, developed by researchers at the National Renewable Energy Laboratory (NREL) and Delft University of Technology (Fleming *et al.,* 2013). The CFD code simulates the wind speed profile behind the 5MW-NREL-reference wind turbine with a rotor diameter of 126m and a hub-height of 90 m (Jonkman *et al*., 2009). The overall coverage and on domain area simulated by the CFD ranges from 0 to 3,000 m in the x- and the y- directions and 0 to 1,000 m in the vertical z-direction. In a 2,394 m ×630 m × 405 m box surrounding the turbines, the discretized meshes with a size of 3 m ×3 m × 3 m in x-, y-, and z- directions are used. We evaluate the wind speed deficit factors $\delta\hat{u}(d,r)$ obtained from CFD results at each grid point on the horizontal x-y plane at the hub height $z = 90\ m$. Figure 6 shows the squared sum errors between the deficit factor obtained from CFD simulation data and the deficit factor computed using the continuous wake model given in Eq. (8) (with $\alpha = 1/3$, $o = 0°$). As shown in the figure, the optimum value $\kappa = 0.033$ minimizing the squared sum is obtained.

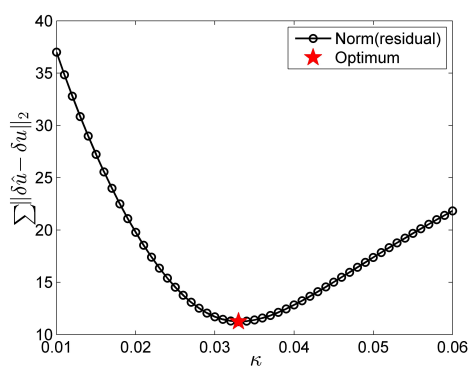

Figure 6. Optimum wake expansion rate

Figure 7(a) compares the deficit factors, at every grid point (d, r) on the horizontal plane $z = 90$ m (hub height), simulated by CFD model and computed from $\delta u(d, r)$ in Eq. (9) with the selected wake expansion rate $\kappa = 0.033$. It can be seen that the continuous wake model describes the variation of the deficit factor inside the wake region reasonably well. By substituting the deficit factor in Eq. (9) with the optimum wake expansion rate $\kappa = 0.033$ into Eq. (4), for a given wind speed U, we can find the wind speed $u(d, r)$ at every grid point (d, r) on the horizontal plane $z = 90$ m (hub height). Figure 7(b) compares the computed wind speed $u(d, r)$ using $U = 8m/s$ to the simulated wind speed profile at different downstream wake distances d varying from $5D$ to $11D$. As shown in Figure 7(b), the variations of wind speeds from the CFD simulation results in both the downstream distance d and radial distance r are well captured by the continuous wake model. This result shows that the continuous wake model using a single wake expansion parameter κ as shown in Eq. (9) can effectively describe the wind speed profile inside the wake formed by an upstream wind turbine.

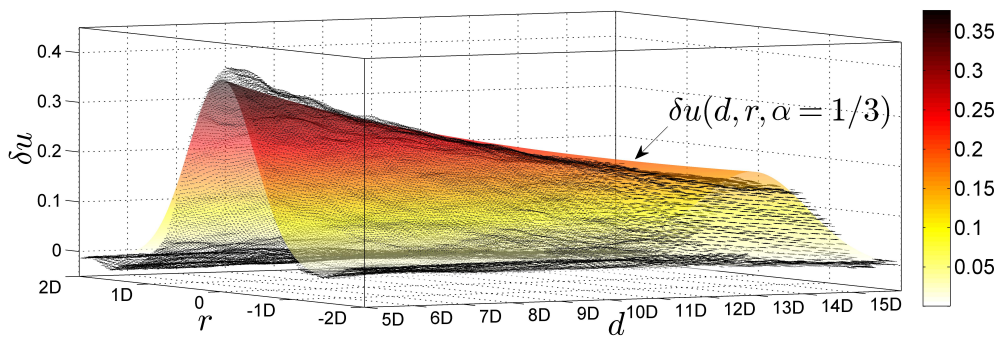

(a) Deficit factors from CFD simulation and Eq. (9) with $\kappa = 0.033$

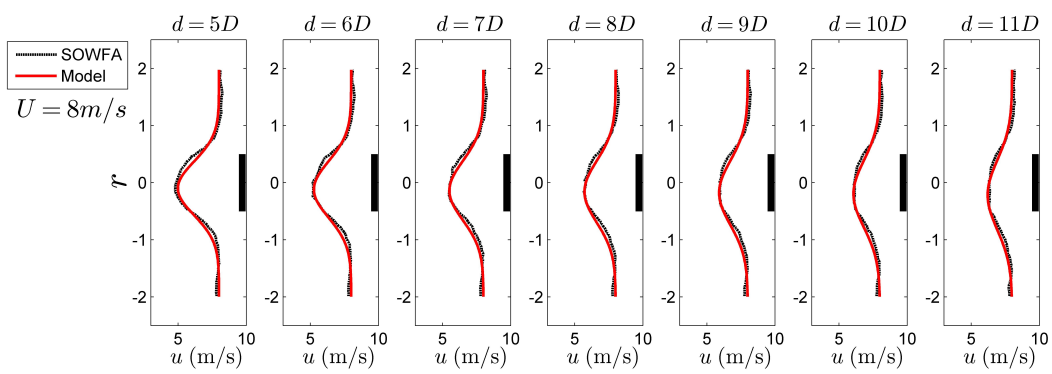

(b) Variations of wind speed profile with downstream wake distance d

Figure 7. Comparisons between the CFD modelled and computed deficit factors and the corresponding wind speed profiles.

Once the wind speed profile inside the wake is constructed, Eq. (17) can now be used to compute the wind turbine power due to the wake-affected wind flow. For validation, we use the power output data simulated using SOWFA for a wind turbine experiencing a wake (Gebraad, *et al*., 2014; Fleming, *et al*., 2014). SOWFA (Churchfield, *et al.*, 2012), which includes an aero-elastic wind turbine response analysis model FAST (Jonkamn and Buhl, 2005), allows the computation of a wind turbine power directly using the CFD simulated wind flow. We compare the calculated wind turbine power by Eq. (17) with the simulated power output data by SOWFA.

With the different radial wake inter distance r_{12} between two wind turbines 1 and 2, as shown in Figure 8(a), the powers from the two wind turbines are computed by the wind farm power function in Eq. (17) and compared to the simulated wind turbine powers by SOWFA. The result shows that the wind farm power function in Eq. (17) underestimates the power from the wind turbine inside the wake (only wind turbine 2). The deviation is possibly caused by the existence of the turbulent flow, sheared wind speed profile, etc., which are omitted during the derviation of wind turbine power based on the actuator disc theory. However, after reducing average deficit factor $\delta\bar{u}$ by 9/10, i.e., $0.9\delta\bar{u}$, we are able to match the power output level reasonable well between the two models, as shown in Figure 8(b). It can also be observed that as the radial wake inter-distance r_{ij} increases, the power of the downstream wind turbine increases due to the reduced wake interference. This phenomenon is captured reasonably well by the wind turbine power function.

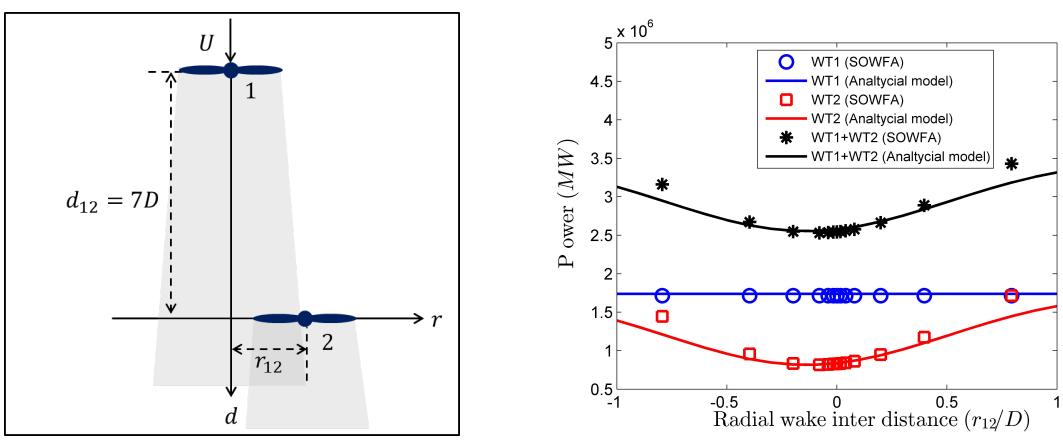

(a) Relative lateral location of two wind turbines (b) Wind farm power with two wind turbines

Figure 8. Variation of wind turbine power production with lateral location of downstream wind turbines.

4. WIND FARM LAYOUT OPTIMIZATION

With the estimated wake expansion rate κ, the proposed power function can describe well the power production of two wind turbines based on their relative locations. Using the continuous wake model, which results in a differentiable power production function, we can now apply a gradient-based optimization algorithm to determine optimal placement of wind turbines that maximizes power production of a wind farm. In this study, we employ sequential convex programming (SCP), which is an efficient method for optimizing non-convex problems, to study the optimal wind farm layout problem. In this section, we first formulate the wind farm layout optimization problem. We then discuss the SCP procedure for the optimization problem.

4.1 Formulation

The wind farm layout problem is to determine the optimal locations $\boldsymbol{l} = \{l_1, \dots, l_{N_T}\}$ of wind turbines that maximize the expected wind farm power production. The optimization problem can be stated as follows:

$$\begin{aligned}
\underset{\boldsymbol{l}}{\text{maximize}} \quad & f(\boldsymbol{l}) = \mathrm{E}\left[\sum_{i=1}^{N_T} P_i(\boldsymbol{l}; U, \theta^W)\right] \\
& = \int_{\theta^W} \int_U \sum_{i=1}^{N_T} P_i(\boldsymbol{l}; U, \theta^W) p(U, \theta^W) dU d\theta^W \\
& = \sum_{k=1}^{N_\theta} \sum_{j=1}^{N_U} \sum_{i=1}^{N_T} P_i(\boldsymbol{l}; U_j, \theta_k^W) \Pr(U_j, \theta_k^W) \\
\text{subject to} \quad & \left\| l_i - l_j \right\|_2 \geq 5D \quad \text{for } i, j = 1, \dots, N_T \ \ (i \neq j) \\
& \underline{\boldsymbol{c}} \leq \mathrm{C}\boldsymbol{l} \leq \overline{\boldsymbol{c}}
\end{aligned} \tag{18}$$

The objective function $f(\boldsymbol{l})$ is the expected wind farm power $\mathrm{E}\left[\sum_{i=1}^{N_T} P_i(\boldsymbol{l}; U, \theta^W)\right]$, where $P_i(\boldsymbol{l}; U, \theta^W)$ is the power of wind turbine i given by Eq.(17) and N_T is the number of wind turbines in a wind farm. The expectation is expressed in terms of the joint probability distribution $p(U, \theta^W)$ of the wind speed U and the wind direction θ^W. Here, the expected wind farm power is approximated as the sum of the power produced by the wind turbines weighted by the joint probability $\Pr(U_j, \theta_k^W)$ for the discrete wind speed U_j and wind direction θ_k^W. Note that N_θ and

N_U are the numbers of bins for the discretization of wind speed U and wind direction θ^W, respectively. The optimization variable $\boldsymbol{l} = (l_i, \dots, l_{N_T})$, where $l_i = (x_i, y_i)$ represents the location vector for wind turbine i, should satisfy two constraints. First, the inter-distance between every pair of two wind turbines should be larger than a specified distance for the safe operation of the wind turbines; in this study, we impose the interdistance constraint $\|l_i - l_j\|_2 \geq 5D$, as shown in Eq. (18), where D is the rotor diameter. Second, each wind turbine is allowed to be located inside a polyhedron described by the constraint $\underline{\boldsymbol{c}} \leq C\boldsymbol{l} \leq \overline{\boldsymbol{c}}$. By specifying the vectors $\underline{\boldsymbol{c}}$ and $\overline{\boldsymbol{c}}$, and matrix C, we can impose various shapes to describe the feasible region for each wind turbine individually. For instance, a feasible region of a rectangular area with widths of w and h for wind turbine i can be expressed as $x_i^0 - (1/2)w \leq x_i \leq x_i^0 + (1/2)w$ and $y_i^0 - (1/2)h \leq y_i \leq y_i^0 + (1/2)h$, where (x_i^0, y_i^0) is the center location of the feasible region. Aggregating the individually imposed feasible region for each wind turbine, the second inequality constraint can be compactly expressed as $\underline{\boldsymbol{c}} \leq C\boldsymbol{l} \leq \overline{\boldsymbol{c}}$ as shown in Eq. (18).

4.2 Sequential Convex Programming

Since the expected wind farm power function $f(\boldsymbol{l})$ and the constraints on the inter distance $\|l_i - l_j\|_2 \geq 5D$ are not concave nor convex, respectively, conventional convex programming cannot be applied directly. This study employs Sequential Convex Programming (SCP) that finds a local optimum of the Eq. (18) by solving a sequence of convex problems that approximate Eq. (18) at each iterate (estimated solution) of the original problem (Fleury, 1993; Boyd, 2014). Given $\boldsymbol{l}^k$, the estimated solution for Eq. (18) at the kth iteration, the iteration proceeds to compute the function value $f^k = f(\boldsymbol{l}^k)$, gradient $\boldsymbol{g}^k = \nabla f(\boldsymbol{l}^k)$ and the hessian matrix B^k, which can then be used to approximate Eq. (18) as a Quadratic Program (QP) stated as follows:

$$
\begin{aligned}
\underset{\boldsymbol{l}}{\text{maximize}} \quad & Q^k(\boldsymbol{l}) \triangleq f^k + (\boldsymbol{l} - \boldsymbol{l}^k)^T \boldsymbol{g}^k + \frac{1}{2}(\boldsymbol{l} - \boldsymbol{l}^k)^T B^k (\boldsymbol{l} - \boldsymbol{l}^k) \\
\text{subject to} \quad & \left(l_i^k - l_j^k\right)^T \left(l_i - l_j\right) > 5D \left\|l_i^k - l_j^k\right\|_2 \text{ for } i, j = 1, \dots, N_T \ \ (i \neq j) \\
& \underline{\boldsymbol{c}} \leq C\boldsymbol{l} \leq \overline{\boldsymbol{c}} \\
& \boldsymbol{l} \in T^k = \{\boldsymbol{l} \mid \|\boldsymbol{l} - \boldsymbol{l}^k\| < \rho^k\}
\end{aligned}
\tag{19}
$$

where $T^k = \{\boldsymbol{l} | \|\boldsymbol{l} - \boldsymbol{l}^k\| < \rho^k\}$, referred to as a trust region, is imposed to guarantee that the solution of Eq. (18) is determined in the region where the approximated quadratic model function $Q^k(\boldsymbol{l})$ is close to the true objective function $f(\boldsymbol{l})$ in Eq. (18). In addition, based on first-order Taylor series expansion at the current solution l_i^k and l_j^k for wind turbines i and j, the inter distance constraint $\|l_i - l_j\|_2 \geq 5D$ between wind turbines i and j is linearized as $(l_i^k - l_j^k)^T (l_i - l_j) > 5D\|l_i^k - l_j^k\|_2$. That is, the locations for wind turbines i and j are constrained with respect to their current solutions l_i^k and l_j^k at the kth iteration.

Figure (9) shows how the feasible region for wind turbine i is defined by the current locations $\boldsymbol{l}^k$ of wind turbines at the kth iteration. First, the feasible region for wind turbine i is shown as the rectangular region subtracted by a circular region representing the prohibited region for wind turbine i imposed by wind turbine j. After the circular prohibited region for wind turbine i due to wind turbine j is linearized into a half space, i.e., one side of a linear function, the feasible region for wind turbine i becomes the rectangular cut off by the half space. Once the linearized prohibited regions by all neighbouring wind turbines are accounted for, as shown in Figure 9, the feasible region for wind turbine i becomes a polyhedron over which its next location is determined by solving Eq. (19).

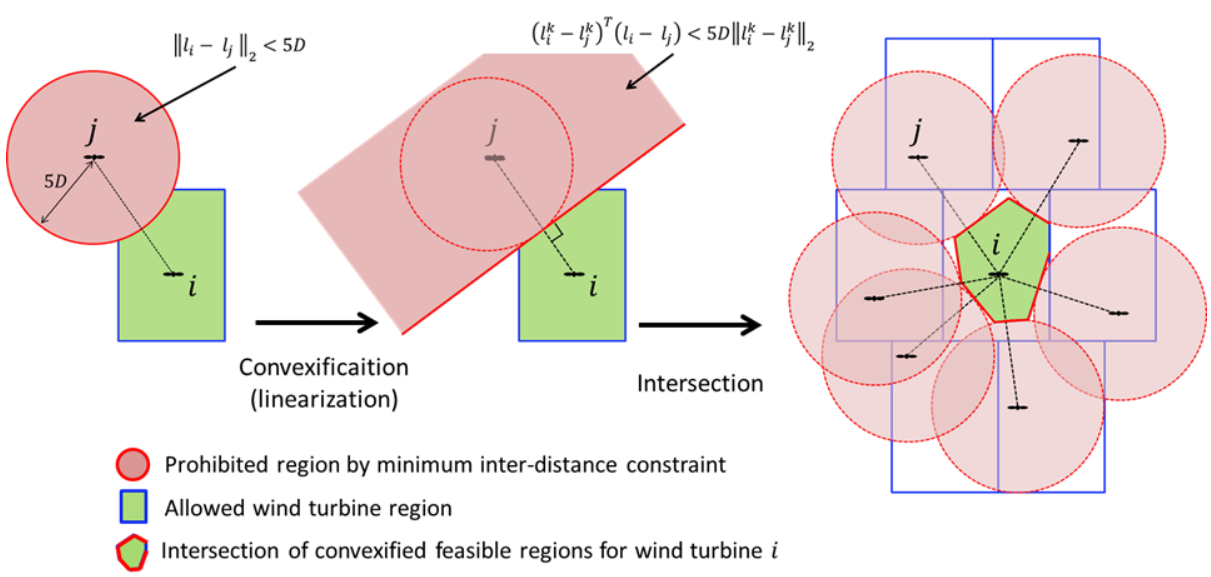

Figure 9: Feasible region for wind turbine i given the current solution $\boldsymbol{l}^k$.

The quadratic program (QP) in Eq. (19) can be solved using CVX, a Matlab based convex programming software (Grant and Boyd, 2013). The SCP algorithm is summarized as shown in Algorithm 1. Let's denote the solution of the QP as $\tilde{\boldsymbol{l}}$. We need to check whether $\tilde{\boldsymbol{l}}$ sufficiently improves the true function $f(\boldsymbol{l})$. If the observed increase $f(\tilde{\boldsymbol{l}}) - f(\boldsymbol{l}^k)$, with respect to the previous function value $f(\boldsymbol{l}^k)$, is larger than a certain threshold ratio γ of the predicted increase $Q^k(\tilde{\boldsymbol{l}}) - f(\boldsymbol{l}^k)$, from the approximate model function $Q^k(\boldsymbol{l})$, the solution $\tilde{\boldsymbol{l}}$ will be used as the next iteration point $\boldsymbol{l}^{k+1}$, and the trust region is expanded as $\rho^{k+1} = \beta\rho^k$ with $\beta > 1$ to expedite the rate for convergence. Otherwise, the current solution $\tilde{\boldsymbol{l}}$ will be rejected, and the trust region will be contracted as $\rho^{k+1} = \beta\rho^k$ with $\beta < 1$ to find a solution nearer the current solution $\boldsymbol{l}^k$. This study uses $\gamma = 0.2$, $\beta = 1.1$ for expansion, and $\beta = 0.5$ for extraction, which are typical values commonly employed using the SCP procedure.

Algorithm 1 Wind farm layout optimization using SCP

initialize (choose) $\boldsymbol{l}^0$
initialize the trust region $T^{(0)} = \{\boldsymbol{l} | \|\boldsymbol{l} - l^0\| < \rho^0\}$
while $\|\boldsymbol{l}^k - \boldsymbol{l}^{k-1}\|_2 < \epsilon$ **do**
    find the solution $\tilde{\boldsymbol{l}}$ by solving Eq. (19)
    if $\frac{f(\tilde{l}) - f(l^k)}{Q^k(\tilde{l}) - f(l^k)} \geq \gamma$ (=0.2 in this study) **then**
        update the solution $\boldsymbol{l}^{k+1} = \tilde{\boldsymbol{l}}$
        assign $\beta > 1$ (typical value = 1.1)
    else
        reject the current solution $\boldsymbol{l}^{(k+1)} = \boldsymbol{l}^{(k)}$
        assign $\beta < 1$ (typical value = 0.5)
    end if
    $\rho^{k+1} = \beta\rho^k$
    increment $k \leftarrow k + 1$
end while

To construct the quadratic model function $Q(\boldsymbol{l})$ in Eq. (19), the gradient $\boldsymbol{g}$ and Hessian matrix B for the objective function $f(\boldsymbol{l})$ are needed. The following describes how these two terms are computed. First, the gradient $\boldsymbol{g}$ of the objective function $f(\boldsymbol{l})$ with respect to $\boldsymbol{l} = \{l_1, \dots, l_{N_T}\} = \{x_1, y_1, \dots, x_{N_T}, y_{N_T}\}$ can be expressed as

$$\boldsymbol{g} = \nabla f = \left(\frac{\partial f}{\partial x_1}, \frac{\partial f}{\partial y_1}, \cdots, \frac{\partial f}{\partial x_q}, \frac{\partial f}{\partial y_q}, \cdots, \frac{\partial f}{\partial x_{N_T}}, \frac{\partial f}{\partial x_{N_T}}\right)^T \tag{20}$$

where

$$\frac{\partial f}{\partial x_q} = \frac{\partial}{\partial x_q}\sum_{k=1}^{N_\theta}\sum_{j=1}^{N_U}\sum_{i=1}^{N_T} P_i\left(\boldsymbol{l}; U_j, \theta_k^W\right)\Pr\left(U_j, \theta_k^W\right) = \sum_{k=1}^{N_\theta}\sum_{j=1}^{N_U}\sum_{i=1}^{N_T}\frac{\partial P_i\left(\boldsymbol{l}; U_j, \theta_k^W\right)}{\partial x_q}\Pr\left(U_j, \theta_k^W\right)$$
$$\frac{\partial f}{\partial y_q} = \frac{\partial}{\partial y_q}\sum_{k=1}^{N_\theta}\sum_{j=1}^{N_U}\sum_{i=1}^{N_T} P_i\left(\boldsymbol{l}; U_j, \theta_k^W\right)\Pr\left(U_j, \theta_k^W\right) = \sum_{k=1}^{N_\theta}\sum_{j=1}^{N_U}\sum_{i=1}^{N_T}\frac{\partial P_i\left(\boldsymbol{l}; U_j, \theta_k^W\right)}{\partial y_q}\Pr\left(U_j, \theta_k^W\right) \tag{21}$$

In Eq. (21), due to the linear combinations of the probability term $\Pr\left(U_j, \theta_k^W\right)$, the partial derivatives are inserted inside the summations.

Denoting $P_i\left(\boldsymbol{l}; U_j, \theta_k^W\right)$ by P_i for simplicity, the term $\partial P_i/\partial x_q$ represents the variation of the power of the ith wind turbine due to the change in the x coordinate of wind turbine q, which can be expressed as

$$\begin{aligned}\frac{\partial P_i}{\partial x_q} &= \frac{\partial P_i}{\partial \bar{u}_i}\frac{\partial \bar{u}_i}{\partial x_q} \\ &= \frac{1}{2}\rho A C_P 3(\bar{u}_i)^2 \mathbf{1}(U_{in} \le \bar{u}_i \le U_{out})\frac{\partial \bar{u}_i}{\partial x_q}\end{aligned} \tag{22}$$

where the derivative $\partial P_i/\partial \bar{u}_i$ has a non zero value $(1/2)\rho A C_P 3(\bar{u}_i)^2$ only when $U_{in} \le \bar{u}_i \le U_{out}$ because, from Eq. (17), P_i is constant regardless of $\bar{u}_i$ when $\bar{u}_i < U_{in}$ or $U_{out} < \bar{u}_i$.

The partial derivative $\partial \bar{u}_i/\partial x_q$ represents the variation of the average wind speed for wind turbine i due to a change in the x coordinate for wind turbine q. As shown in Eqs. (15) and (16), $\bar{u}_i$ is a function of the locations $\boldsymbol{l}$ of all wind turbines. The partial derivative can be computed using chain rule as

$$\frac{\partial \bar{u}_i}{\partial x_q} = \sum\nolimits_{k=1, k\neq i}^{N_T}\frac{\partial \bar{u}_i}{\partial \delta \bar{u}_{ik}}\frac{\partial \delta \bar{u}_{ik}}{\partial x_q} \tag{23}$$

In Eq. (23), the first term $\partial \bar{u}_i/\partial \delta \bar{u}_{ik}$ inside the summation can be computed using Eqs. (15) and (16). The second term in the summation $\partial \delta \bar{u}_{ik}/\partial x_q$ represents how the average deficit factor for wind turbine i due to wake effect

from wind turbine k varies by a change in the x coordinate for wind turbine q. There are two possible cases when computing the derivative $\bar{u}_{ik}/\partial x_q$:

(1) When $q = i$: the derivatives $\partial\delta\bar{u}_{ik}/\partial x_q = \partial\delta\bar{u}_{ik}/\partial x_i$ are non-zero for any free index k except for $k \neq i$. In other words, as wind turbine i moves, its average deficit factor is influenced by other wind turbine $k = 1, \dots, N_T, k \neq i$.

(2) When $q \neq i$: the derivatives $\partial\delta\bar{u}_{ik}/\partial x_q$, for $k = 1, \dots, N_T$, are zero except for $\partial\delta\bar{u}_{iq}/\partial x_q$ when $k = q$. In this case, the gradient only accounts for how the change in x_q of wind turbine q affects the average deficit factor $\delta\bar{u}_{iq}$ of wind turbine i.

The terms $\partial\delta\bar{u}_{ik}/\partial x_i$ and $\partial\delta\bar{u}_{ik}/\partial x_q$ can be computed using the continuous wake equations described in Section 2.

To approximate the Hessian matrix B^{k+1}, we use the observed gradients at two successive iterations using the relationship of $B^{k+1} = (\boldsymbol{g}^{k+1} - \boldsymbol{g}^k)/(\boldsymbol{l}^{k+1} - \boldsymbol{l}^k)$. Setting $\boldsymbol{z}^k \triangleq \boldsymbol{l}^{k+1} - \boldsymbol{l}^k$ and $\boldsymbol{y}^k \triangleq \boldsymbol{g}^{k+1} - \boldsymbol{g}^k$, the update for B^{k+1} can be determined as a rank-two update to the previous B^k as (Nocedal and Wright, 2000):

$$B^{k+1} = B^k - \frac{B^k \boldsymbol{z}^k (\boldsymbol{z}^k)^T B^k}{(\boldsymbol{z}^k)^T B^k \boldsymbol{z}^k} + \frac{\boldsymbol{y}^k (\boldsymbol{y}^k)^T}{(\boldsymbol{y}^k)^T \boldsymbol{z}^k} \tag{24}$$

Note that the solution of the QP in Eq. (19) is well defined only when B^k is negative semi-definite, which guarantees that $Q^k(\boldsymbol{l})$ is a concave function. To ensure that Eq. (19) is well defined, we use the "damped" BFGS update method, for which $\boldsymbol{y}^k$ in Eq. (24) is replaced by the "damped" gradient change $\boldsymbol{r}^k$ defined as (Nocedal and Wright, 2000)

$$\boldsymbol{r}^k = \lambda^k \boldsymbol{y}^k + (1 - \lambda^k) B^{k-1} \boldsymbol{z}^k \tag{25}$$

where

$$\lambda^k = \begin{cases} 1 & \text{if } (\boldsymbol{z}^k)^T \boldsymbol{y}^k \geq 0.2 (\boldsymbol{z}^k)^T B^k \boldsymbol{z}^k \\ \dfrac{0.8 (\boldsymbol{z}^k)^T B^k \boldsymbol{z}^k}{(\boldsymbol{z}^k)^T B^k \boldsymbol{z}^k - (\boldsymbol{z}^k)^T \boldsymbol{y}^k} & \text{if } (\boldsymbol{z}^k)^T \boldsymbol{y}^k < 0.2 (\boldsymbol{z}^k)^T B^k \boldsymbol{z}^k \end{cases} \tag{26}$$

Although other combinations are possible, the constants of 0.2 and 0.8 shown in Eq. (26) are typical values that are commonly used to compute λ^k (Nocedal and Wright, 2000).

5. APPLICATION TO WIND FARM SITE

In this section, we apply the layout optimization procedure to study the configuration of a wind farm. Specifically, the layout of Horns Rev 1 wind farm, located in Denmark, is selected because of the availability of data of the wind farm site (Tech-wise, 2002). The expected wind farm output is constructed using statistical data on the wind direction and speed at the site. The initial configuration is taken to be the current locations of the wind turbines. The objective is to determine the optimal locations of the wind turbines to see whether the wind farm power efficiency can be further improved. The purpose of this study is not to suggest relocating the wind turbines but to gain insight into the optimum wind farm layout problem given the wind conditions at the site. We assume that the wind turbines are represented by the wind turbine model described in the previous sections. Note that the study focuses on the relative power efficiency of a wind farm, which, in theory, does not depend on specific types of wind turbines. Optimization results are also obtained for different wake expansion rate κ to assess the optimization layouts at different terrain (i.e., surface roughness) conditions. Figure 10 shows the configuration of the Horns Rev1 wind farm, in which 80 wind turbines are arranged in a grid pattern. The wind turbines are laid in the shape of a rhombus where the separating distance along the two sides and the diagonal are, respectively, $7D$ and $10.4D$, where D is the diameter of a wind turbine rotor.

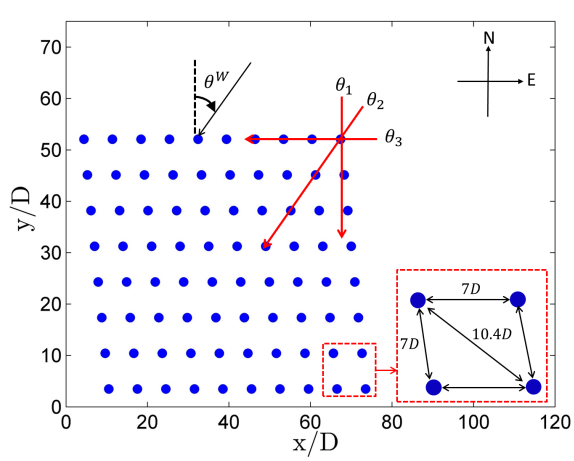

Figure 10: Wind turbine layouts

5.1 Layout optimization for a single wind direction

For different wind directions θ^W varying from 0° to 360°, with an increment of 1°, and at the fixed wind speed $U = 8m/s$, we compute the power efficiency of the target wind farm using the locations of wind turbines, denoted as the initial solution $\boldsymbol{l}^0$, in the target site. The power efficiency of the wind farm given the wind turbine location $\boldsymbol{l}$, wind direction U and wind direction θ^W, can be expressed as

$$\eta(\boldsymbol{l}; U, \theta^W) = \frac{\sum_{i=1}^{N_T} P_i(\boldsymbol{l}; U, \theta^W)}{N_T P^*(U)} \tag{27}$$

where $P^*(U)$ denotes the power of each of the $N_T(= 80)$ wind turbines in the wind farm assuming there is no wake interference. The expression for $P^*(U)$ is given by Eq. (3). Figure 11 shows how $\eta(\boldsymbol{l}^0; U = 8m/s, \theta^W)$ varies as the wind direction θ^Wchanges. As shown in the figure, the wind farm power efficiency varies depending on the wind direction θ^W and can be quite inefficient at certain wind directions, for examples when $\theta^W = 0°, 41°$ and 90°, defined, respectively, as θ_1, θ_2, and θ_3 as shown in Figure 10.

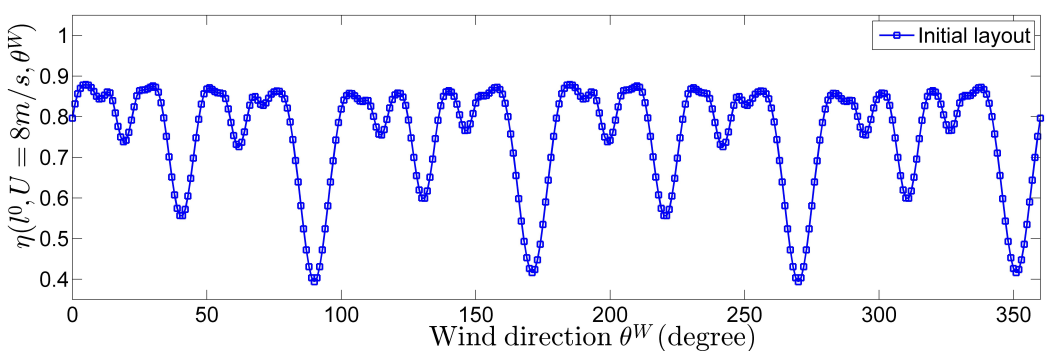

Figure 11: Variation of wind farm power efficiency with wind direction

Taking the layout shown in Figure 10 as the initial configuration of the wind turbines, we apply SCP to find the locations that maximize the power efficiency of the wind farm $\eta(\boldsymbol{l}; U = 8m/s, \theta^W)$ for three wind directions $\theta^W = 0°, 41°$ and 90°. Figure 12 shows the initial and the optimized locations of the wind turbines, depicted, respectively, as solid squares and solid circles in the figure. The trajectory shows the changes of the wind turbine locations with the iterations of the SCP. The shaded circles around the optimized locations represent the prohibited

regions by the minimum inter distance constraints among the wind turbines. Furthermore, all the wind turbines are constrained to be located within the boundary of the current wind farm (global feasible region constraint) so that the wind farm power efficiencies can be compared for a given wind farm area. Given a wind direction, the wind turbines move collectively in a certain pattern to minimize the wake interference. The wind turbines are relocated with respect to the direction of coming wind flow to enable the wind turbines at the downstream to be affected less by wakes by the upstream wind turbines. Table 1 summarizes the increase in wind farm efficiency for the optimized locations due to wind directions $\theta^W = 0°, 41°$ and $90°$.

As shown in Table 1, with the wind direction $\theta^W = 0°$, from the North, the optimal layout improves the power production efficiency by about 10%. For the case of $\theta^W = 41°$, an improvement of about 56% is achieved comparing to initial layouts that suffers relatively high wake influence from the upstream wind turbines. To optimize the power production, the wind turbines are scattered around to avoid the alignment between the wind direction and the wind turbine arrays. Note that, as shown in Fig 12(b), the wind turbines move collectively in the clockwise direction while fully exploiting the allowed wind farm area. For the case of $\theta^W = 90°$ where the wind flow coming from the eastern direction, the wind turbine arrays are initially parallel to the wind flow; as a result, the wake is intensified as multiple wakes are merged within a long sequence of wake chains. The intensified wake significantly lowers the power production of the downstream wind turbines. As shown in Figure 12(c), wind turbines are relocated in diagonal wind turbine arrays to avoid wakes flowing from the east to west. As a result, as shown in Table 1, the wind farm power efficiency improves over 100%.

Table 1: Improvements on wind farm power efficiency by SCP

	$\eta(\boldsymbol{l}^0; U = 8m/s, \theta^W)$	$\eta(\boldsymbol{l}^*; U = 8m/s, \theta^W)$	$\frac{(\eta(\boldsymbol{l}^*,\theta^W)-\eta(\boldsymbol{l}^0,\theta^W))}{\eta(\boldsymbol{l}^0,\theta^W)} \times 100$ (%)
$\theta_W = \theta_1 (= 0°)$	0.828	0.913	10.273
$\theta_W = \theta_2 (= 41°)$	0.583	0.908	55.823
$\theta_W = \theta_3 (= 90°)$	0.432	0.873	101.951

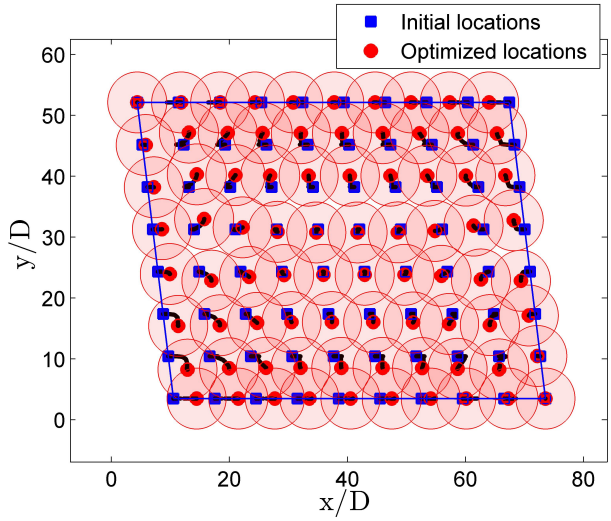

(a) $\theta^W = \theta_1 (= 0°)$

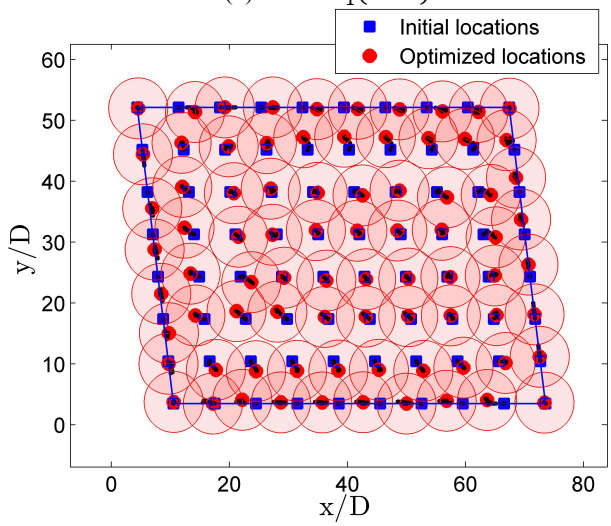

(b) $\theta^W = \theta_2 (= 41°)$

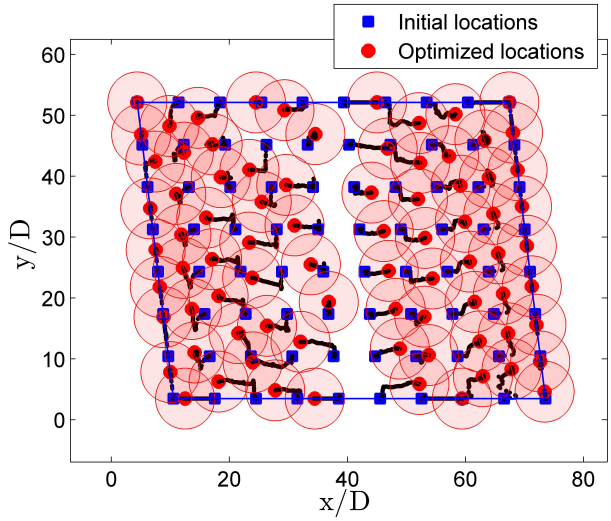

(c) $\theta^W = \theta_3 (= 90°)$

Figure 12: Optimized wind turbine locations for different wind direction θ^W

5.3 Expected wind farm power maximization

In the previous section, we show that the layout optimization can effectively improve the power efficiency of a wind farm for a given wind condition (i.e., a single wind speed and direction). In general, however, the wind flow speed and direction vary. To account for the variability in the wind direction and the wind speed at a target site, we construct the expected wind farm power function using the distributions of the wind direction and the wind speed at the given wind farm site. The objective is thus to determine the optimum wind farm layout that maximizes the expected wind farm power production. To obtain the expected wind farm power function, we utilize the information about the wind condition at the site.

Table 2 summarizes the statistical parameters of the wind direction and the wind speed distributions computed from the wind data collected from May 1999 to October 2002 at the Horns Rev 1 wind farm (Tech-wise, 2002). The parameters effectively describe the wind characteristics of the target site. First, the probability mass function $\Pr(\theta_k^W)$ for the discretized wind directions θ_k^W, with $k = 1, \dots, 12$, describes the relative occurrence of the wind direction θ_k^W at the site. Specifically, $\Pr(\theta_k^W)$ represents the probability that the wind direction θ^W belongs to the kth wind direction bin θ_k^W with an interval of $\pm 15°$. Figure 13(a) represents $\Pr(\theta_k^W)$ as a circular histogram; a vertex of the polyhedron indicates the direction of wind flow and the length between the center and the vertex represents the probability of the wind direction. Second, the wind speed distribution $\mathrm{PDF}(U|\theta_k^W)$ conditional on wind direction θ_k^W is modelled using the Weibull distribution as

$$\mathrm{PDF}(U|\theta_k^W) = \begin{cases} \dfrac{\Gamma_k}{\lambda_k}\left(\dfrac{U}{\lambda_k}\right)^{(\Gamma_k - 1)} \exp\left(-\left(\dfrac{U}{\lambda_k}\right)^{\Gamma_k}\right) & U \geq 0 \\ 0 & U < 0 \end{cases} \tag{28}$$

where Γ_k and λ_k are the shape factor and the scale factor of the distribution, respectively. The continuous wind speed distribution given a wind direction θ_k^W can be compactly represented by the parameters Γ_k and λ_k. The probability $\Pr(\theta_k^W)$ and the parameters Γ_k and λ_k for $\mathrm{PDF}(U|\theta_k^W)$ for $k = 1, \dots, 12$ are shown in Table 2 (Tech-wise, 2002). Figure 13(b) shows the $\mathrm{PDF}(U|\theta_k^W)$, $k = 1, \dots, 12$, for the 12 bins of wind directions.

Table 2: Statistical wind data at the target site (Tech-wise, 2002).

k	θ_k^W	$\Pr(\theta_k^W)$	$\mathrm{PDF}(U\|\theta_k^W)$	
			Shape factor Γ_k	Scale factor λ_k
1	0°	0.051	8.65	2.11
2	30°	0.043	8.86	2.05
3	60°	0.044	8.15	2.35
4	90°	0.066	9.98	2.55
5	120°	0.089	11.35	2.81
6	150°	0.065	10.96	2.74
7	180°	0.087	11.28	2.63
8	210°	0.115	11.50	2.40
9	240°	0.121	11.08	2.23
10	270°	0.111	10.94	2.28
11	300°	0.114	11.27	2.29
12	330°	0.096	10.55	2.28

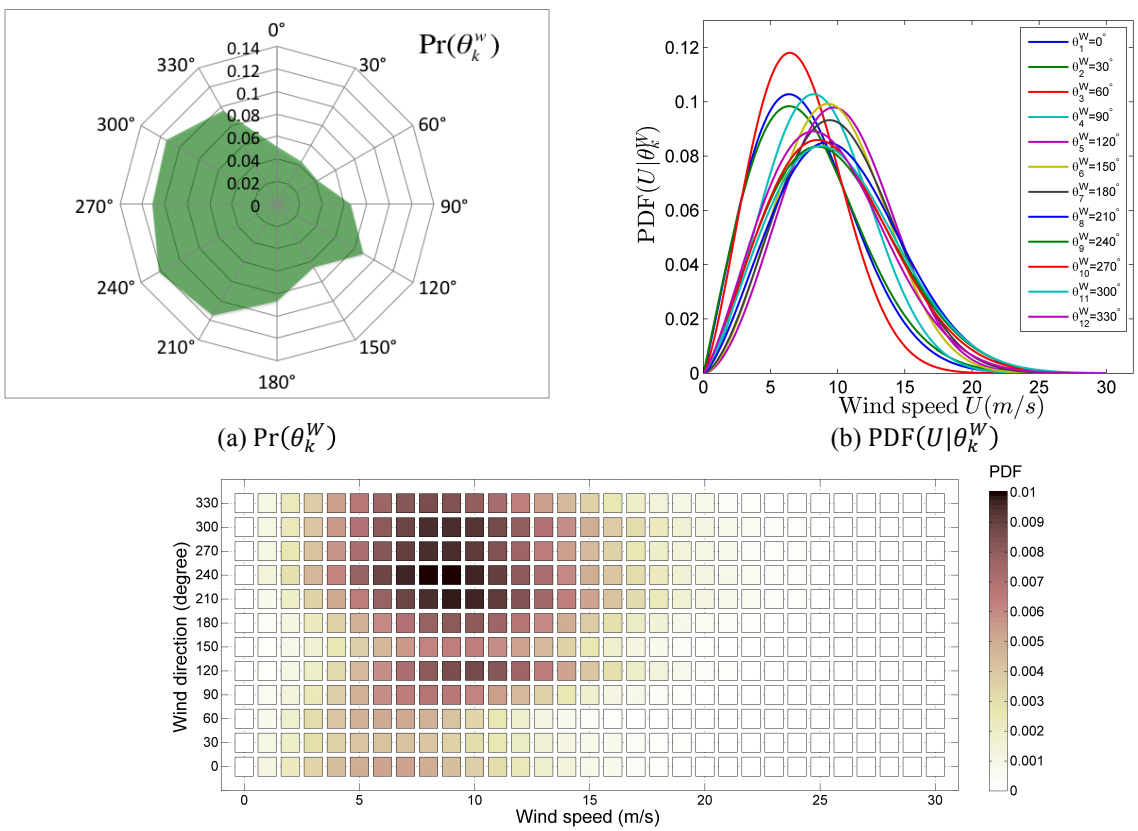

(a) $\Pr(\theta_k^W)$ (b) $\mathrm{PDF}(U|\theta_k^W)$

(c) $\Pr(U_j, \theta_k^W) = \Pr(U_j|\theta_k^W)\Pr(\theta_k^W)$

Figure 13: Wind condition at the target site

From the continuous probability density function $\mathrm{PDF}(U|\theta_k^W)$, the probability mass function $\Pr(U_j|\theta_k^W)$ for the discretized wind speed U_j can be computed. By combining the probability mass function $\Pr(\theta_k^W)$ for the wind direction θ^W and the probability mass function $\Pr(U_j|\theta_k^W)$ for the discretized wind speed U conditional on the wind direction θ^W, the joint probability mass function for U and θ^W can then be computed as $\Pr(U_j, \theta_k^W) = \Pr(U_j|\theta_k^W)\Pr(\theta_k^W)$. Figure 13(c) shows the 2-D histogram plot for the constructed $\Pr(U_j, \theta_k^W)$. Substituting $\Pr(U_j, \theta_k^W) = \Pr(U_j|\theta_k^W)\Pr(\theta_k^W)$ in Eq. (18), the expected wind farm power at the target site can be expressed as

$$\begin{aligned} \mathrm{E}\left[\sum_{i=1}^{N_T} P_i(\boldsymbol{l}; U, \theta^W)\right] &= \sum_{k=1}^{N_\theta}\sum_{j=1}^{N_U}\sum_{i=1}^{N_T} P_i(\boldsymbol{l}; U_j, \theta_k^W)\Pr(U_j, \theta_k^W) \\ &= \sum_{k=1}^{N_\theta}\Pr(\theta_k^W)\sum_{j=1}^{N_U}\Pr(U_j|\theta_k^W)\sum_{i=1}^{N_T} P_i(\boldsymbol{l}; U_j, \theta_k^W) \end{aligned} \tag{29}$$

Eq. (29) is the objective function to be maximized in terms of the location variable $\boldsymbol{l}$. The expected wind farm power efficiency can be defined as

$$\bar{\eta}(\boldsymbol{l}) = \frac{\sum_{k=1}^{N_\theta}\sum_{j=1}^{N_U}\sum_{i=1}^{N_T} P_i(\boldsymbol{l}; U_j, \theta_k^W)\Pr(U_j, \theta_k^W)}{N_T\left(\sum_{k=1}^{N_\theta}\sum_{j=1}^{N_U} P^*(U_j)\Pr(U_j, \theta_k^W)\right)} \tag{30}$$

where the denominator is the expected wind farm power that can be produced assuming no wake interference at the wind turbines.

Figure 14(a) shows the optimized wind turbine locations that maximize the expected wind farm power. The initial layout of the wind farm as shown in Figure 10 is employed as the initial solution. During the optimization, as shown in the Figure 14(a), the wind turbines are shifted slightly from their initial locations. Figure 14(b) shows the increase in the wind farm power efficiency from 83.6% to 89.8% as the iteration proceeds. Note that the initial wind farm power efficiency of 83.6% estimated by Eq. (30) using $\boldsymbol{l}^0$ is comparable to the measured power efficiency at the wind farm site and the estimated by the wind farm power evaluation software (Ott and Nielsen, 2014). We should also note that the incremental improvement in the wind farm power efficiency and the convergence, shown in Figure

14(b), illustrate the applicability of SCP with the analytically derived gradient function for the wind farm layout optimization problem.

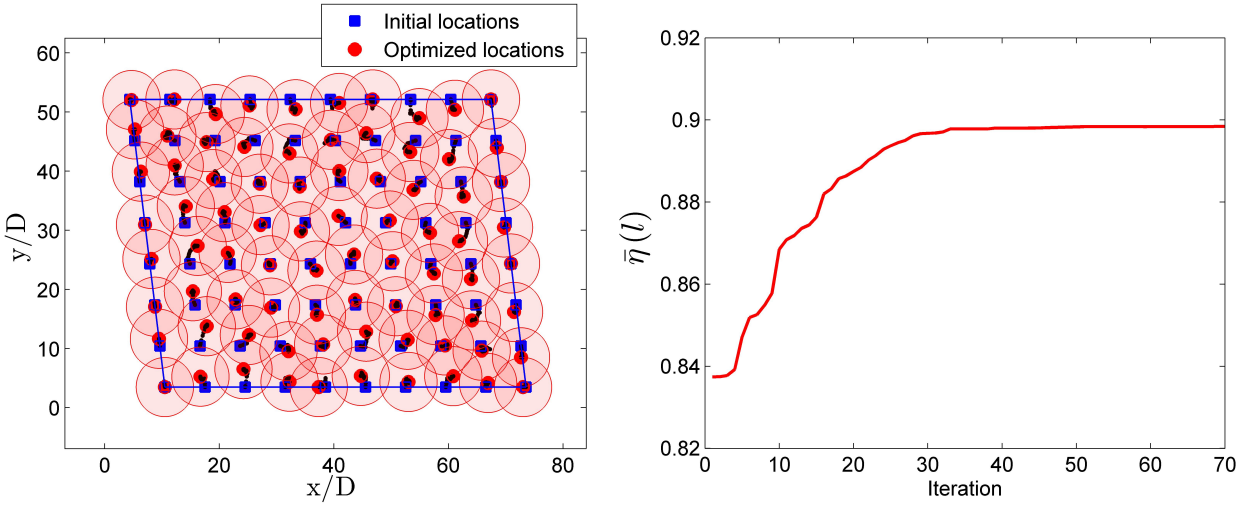

(a) Optimized wind turbine locations (b) Optimized wind farm power efficiency

Figure 14: Optimized wind turbine locations considering distributions of wind directions and speeds.

Figure 15 shows the sensitivity of the expected wind farm power efficiency of the optimized layout with respect to the wind direction. As noted earlier and shown in Figure 15, the effect of wind direction can be quite significant for the initial layout particularly when $\theta^W = 90°$ or $270°$ where wind blows parallel to the wind turbine arrays. For the optimized wind farm, however, the level of variation is significantly reduced, and the decrease in power production at $\theta^W = 90°$ and $270°$, is significantly less. The reduced sensitivity and the increased efficiency are mainly due to a scattered wind turbine placement shown in Figure 14(a). Because the scattered wind turbine configuration, compared to the latticed wind turbine configuration, effectively prevents the formation of a long sequence of wake chains, the optimized configuration makes the downstream wind turbines experiencing less intensified wake. The steady wind farm power production for different wind directions could be beneficial for operating a large-scale wind farm. It should be noted that the expected wind farm power is computed using 12 discretized wind direction bins and the associated wind speed distribution. If more detailed statistical wind data is available, the estimation on expected wind farm power can be further refined.

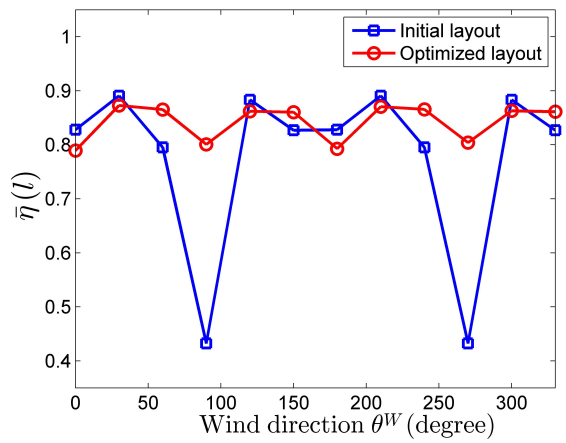

Figure 15:Variations of expected wind farm power efficiency due to wind directions.

5.4 Influence of the wake expansion rate

The wake expansion rate κ varies depending on the terrain condition for a wind farm site. The wake expansion rate κ determines how a wake expands as it propagates in the downstream direction, thereby affecting the intensity of the wake. Accordingly, the wake expansion rate κ affects the expected wind farm power efficiency. For different values of κ, Figure 16(a) compares the changes in the expected wind farm power efficiency from the optimization results. As shown in the figure, the lower κ values result in lower wind farm power efficiencies in general because the narrow and intensified wake associated with the lower κ values significantly lower the wind farm power produced by the downstream wind turbines. As κ increases, on the other hand, the wake disperses wider with less interference on downstream wind turbines; therefore, the overall expected wind farm power efficiency increases.

The wake expansion rate κ affects the improvement of the expected wind farm power efficiency obtained for the optimal layouts. As shown in the Figure 16(b), the improvement rate decreases as κ increases. The lower κ value results in a narrower wake region and provides a larger space for the wind turbines to relocate and to escape from the wakes. As the wake region becomes wider as κ increases, however, relocating wind turbines to avoid the wakes becomes more difficult. Table 3 summaries the relative improvements in the expected wind farm power efficiency by the optimised wind farm layout for different values of κ.

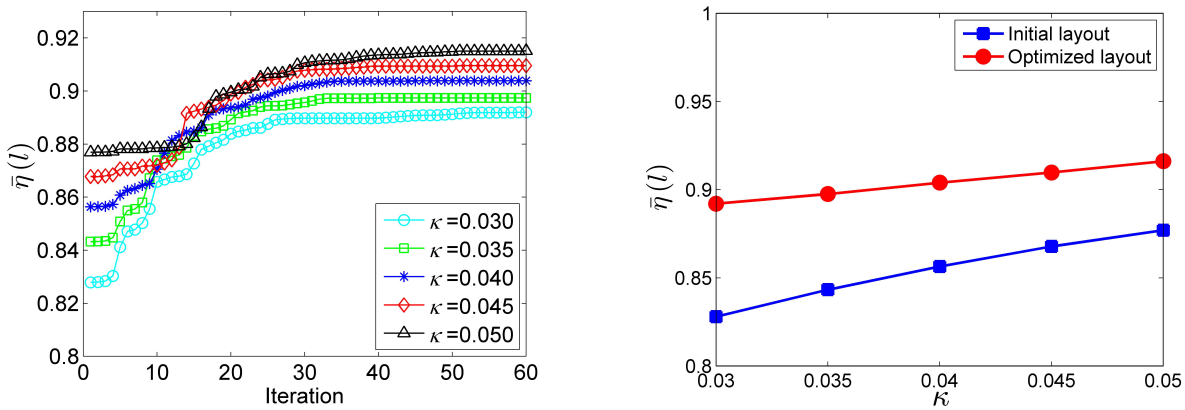

(a) Iteration results using SCP (b) Improvement by layout optimization

Figure 16: Influence of wake expansion rate κ on expected wind farm power efficiency

Table 3: Influence of wake expansion rate κ on expected wind farm power efficiency

Wake expansion rate κ	Initial $\bar{\eta}(\boldsymbol{l}^0)$	Improved $\bar{\eta}(\boldsymbol{l}^*)$	Relative improvement rate $\frac{\left(\bar{\eta}(\boldsymbol{l}^*)-\bar{\eta}(\boldsymbol{l}^0)\right)}{\bar{\eta}(\boldsymbol{l}^0)}\times 100\ (\%)$
0.030	0.828	0.892	7.748
0.035	0.843	0.898	6.437
0.040	0.856	0.904	5.555
0.045	0.868	0.910	4.832
0.050	0.877	0.916	4.464

6. DISCUSSION AND CONCLUSION

This study demonstrates the use of mathematical optimization to determine the optimum wind farm configuration that maximizes the expected wind farm energy production. First, we derive the continuous wake model to accurately describe the wind speed profile inside the wake formed behind the upstream wind turbine. Specifically, we use a Gaussian function to describe the continuous variation of wind speed in the radial direction of the wake. The proposed continuous wake model compares favourably with the variation of wind speed inside a wake simulated by CFD. Using the wake model, the wind farm power function is then constructed as a differentiable function of wind turbine location variables. The optimum configuration of a wind farm is determined by maximizing the wind farm power function in terms of wind turbine location variables. By exploiting the differentiability of the wind farm power function, we determine the gradient and Hessian matrix and employ Sequential Convex Programing (SCP) to

maximize the objective function. SCP is scalable to solve a wind farm layout problem even with larger number of wind turbines.

For illustration, the proposed wind farm power function and the optimization strategy are applied to evaluate the efficiency of Horns Rev 1 wind farm. The results reveal that the power efficiency of the wind farm varies significantly depending on wind directions. Through optimization, insights can be gained about the configuration of wind turbines that is beneficial for mitigating wake interference. For instance, when the wind turbines are scattered with respect to incoming wind flow, the long sequence of wake chain is prevented and, thus, the powers of downstream wind turbines are not affected significantly. Furthermore, we construct the expected wind farm power function by incorporating the statistical data about the wind condition at the target site to quantify the overall wind farm power production. We then maximize the expected wind farm power to determine the optimum wind farm configuration that statistically maximizes wind farm power over a long period. The result shows that the scattered placements of wind turbines increase the expected wind farm power by 7.3%. Additionally, the optimized layout decreases the sensitivity of the wind farm power with respect to the variation in wind direction. To study how different characteristics of a wind farm site may influence power production, we investigate the effects of the wake expansion rate on the wind farm power. When the wake expansion is low, the wind farm power efficiency are generally low due to highly intensified wake interference, but optimized layout can improve the wind farm power efficiency.

While employing iterative gradient-based optimization method, such as SCP employed in this study, the algorithm finds not the global optimum but one of local optimums. Therefore, it is important to ensure that a local optimum value is close to the global maximum (although it is unknown). To this end, a wind farm configuration designed using conventional standard can be used as the initial solution for SCP. Since SCP incrementally improves the objective value, the optimized configuration by SCP is guaranteed to improve the objective value compared to the initial wind farm configuration. For example, we can collect a set of possible wind farm configurations that result in reasonably high wind farm power using conventional design approach. For each wind farm configuration, SCP can be employed to improve the wind farm power efficiency. The wind farm configuration with the best resultant wind farm power efficiency can then be selected as the final design.

Various types of data can now be collected to construct the expected wind farm power function so that the formulated wind farm layout problem applies to a specific target wind farm site. In this study, CFD simulation data on the wind speed inside a wake is used to calibrate the wake model. The wind turbine power data simulated by the wind turbine analysis code is used to calibrate the power function of a wind turbine. The statistical data on wind speed and wind direction are used to construct the expected wind farm power function. With abundant contextualized data collected from a wind farm site, we can gain valuable insights into the interactions among wind turbines in wind farm and their influences on the wind farm power. This study illustrates how these data can be beneficially incorporated in developing optimization strategy for designing the configuration of an efficient wind farm in terms of power production.

ACKNOWLEDGEMENT

The authors would like to thank Dr. P.M.O. Gebraad and Dr. P.A. Fleming from the National Renewable Energy Laboratory (NREL), and Dr. J.W. van Wingerden at Delft University of Technology, who provided the simulated data of the wind speed profile behind a 5MW-NREL-reference wind turbine and the data on the computed power of the wind turbine located inside the wake (Gebraad, *et al*., 2014; Fleming, *et al*., 2014)

REFERENCE

Ainslie, J. P. (1988). "Calculating the flow field in the wake of wind turbines," *Journal of Wind Engineering and Industrial Aerodynamics*, 27, 213-224.

AWS Truepower. (2008). OpenWind [Software]. Albany, NY, USA.

Bartl, J. (2011). "Wake measurement behind an array of two model wind turbines," M.S. Thesis, Royal Institute of Technology, Stockholm, Sweden.

Betz, A. (1966). "Introduction to the theory of flow machines," Pergamon Press.

Bilbao, M. and Alba, E. (2009). "Simulated annealing for optimization of wind farm annual profit," *2nd International symposium on logistics and industrial informatics*, Linz, Austria.

Boyd, S. (2014). "Sequential Convex Programming," [Online lecture notes], Retrieved from: http://www.stanford.edu/class/ee364b/lectures/seq slides.pdf

Chowdhury, S., Zhang, J., Messac, A. and Castillo, L. (2012). "Unrestricted wind farm layout optimization: investigating key factors influencing the maximum power generation," *Renewable Energy*, 38, pp. 16–30.

Chowdhury, S., Zhang, J, Messac, A. and Castillo, L. (2013). "Optimizing the arrangement and the selection of turbines for a wind farm subject to varying wind conditions," *Renewable Energy*, 52, pp. 273-282.

Churchfield, M. J., Lee, S., Michalakes, J., and Moriarty, P. J. (2012). "A Numerical Study of the Effects of Atmospheric and Wake Turbulence on Wind Turbine Dynamics," *Journal of Turbulence*, 13(14), pp. 1-32.

DNV GL. (2014). WindFarmer [Software]. Høvik, Norway.

Du Pont, B. and Cagan, J. (2012). "An extended pattern search approach to wind farm layout optimization," *Journal of Mechanical Design*, 134.

Elkinton CN, Manwell JF, McGowan JG. (2008). "Algorithms for offshore wind farm layout optimization," *Wind Engineering*, 32(1), pp. 67-84.

EMD International. (2011). WindPro [Software]. Aalborg, Denmark.

Eroglu, Y and Seckiner, SU. (2012). "Design of wind farm layout using ant colony algorithm," *Renewable Energy*, 44, pp. 53-62.

Fleming, P., Lee, S., Churchfield, M., Scholbrock, A., Michalakes, J., Johnson, K.,…Wingerden, P. (2013). "The SOWFA Super-Controller: A high-fidelity tool for evaluating wind plant control approaches," EWEA 2013.

Fleming, P., Gebraad, P, Lee, S., Wingerden, J., Johnson, K., Churchfield, M.,…Moriarty, P. (2014). "Simulation comparison of wake mitigation control strategies for a two-turbine case," *Wind Energy,* DOI: 10.1002/we.1810.

Fleury C. (1993). "Sequential convex programming for structural optimization problems," Optimization of large structural systems, 1, pp. 531–53.

Gebraad, P., Teeuwisse, F., Wingerden, J., Fleming, P., Ruden, S., Marden, J., Pao, L. (2014). "A data-driven model for wind plant power optimization by yaw control," *Proc. American Control Conference 2014,* Portland, U.S.

Grady, S. A., Hussaini, M. Y. and Abdullah, M. M. (2005). "Placement of wind turbines using genetic algorithms", *Renewable Energy*, 30(2), pp. 259-270.

Grant, M and Boyd, S. (2014). The CVX User's Guide 2.0. CVX Research, INC., 2013.

Jensen, N. O. (1983). "A Note on Wind Generator Interaction," Tech. Rep. Risø-M2411(EN), Risø National Laboratory.

Jonkman, J., Butterfield, S., Musial, W., and Scott, G. (2009). "Definition of a 5-MW reference wind turbine for offshore system development," Technical Report NREL/TP-500-38060, National Renewable Energy Laboratory.

Jonkman, J., Buhl., M. (2005). "FAST User's Guide," Technical Report, NREL/EL-500-38230.

Katic, I., Hojstrup, J. and Jensen, N. (1986). "A simple model for cluster efficiency," *Proc. of European Wind Energy Association Conference and Exhibition*, pp. 407–410.

Kusiak, A. and Song, Z. (2010). "Design of wind farm layout for maximum wind energy capture," *Renewable* Energy, 35, pp. 685–694.

Marmidis, G., Lazarou S. and Pyrgioti E. (2008). "Optimal placement of wind turbines in a wind park using Monte Carlo simulation," *Renewable Energy*, 33, pp. 1455-1460.

Mosetti, G., Poloni, C. and Diviacco, B. (1994). "Optimization of wind turbine positioning in large wind farms by means of a genetic algorithm," *Journal of Wind Engineering and Industrial Aerodynamics*, 51, pp. 105-116.

Nocedal, J. and Wright, S. (2000). "Numerical Optimization," Springer.

Ott, S. and Nielsen, M. (2014). "Developments of the offshore wind turbine wake model Fuga," DTU Wind Energy E-0046.

Risø. (2011). WasP [Software]. Roskilde, Denmark.

Serrano J, González AG, Castro J, Riquelme J, Burgos M. (2010). "Optimization of wind farm turbines layout using an evolutive algorithm," *Renewable Energy*, 35, pp. 1671-1681.

Salcedo-Sanz et al. (2014). "Offshore wind farm design with the coral reefs optimization algorithm," *Renewable Energy*, 63, pp. 109-115.

Tech-wise. (2002). "Wind Resources at Horns Rev, Tech Report, Eltra PSO-2000.

Wan, C., Wang, J., Yang, G., Gu, H. and Zhang, X. (2012). "Wind farm micro-sitting by Gaussian particle swarm optimization with local search strategy," *Renewable Energy*, 48, pp. 276-286.